Proceedings of Global Power and Propulsion Society
ISSN-Nr: 2504-4400
Beijing Conference 2019
16th – 18th September, 2019
www.gpps.global

GPPS-BJ-2019-215

Turbulent Flow Simulation for a Sharp Immersed Boundary Method

Congcong Chen
chencongcong@buaa.edu.cn
Beijing, China

Zhuo Wang
wzhuo@buaa.edu.cn
Beijing, China

Lin Du
lindu@buaa.edu.cn
Beijing, China

Xiaofeng Sun
sunxf@buaa.edu.cn
Beijing, China

ABSTRACT

In this paper, a wall function is combined with the sharp immersed boundary method (IBM) for turbulent flow simulation on Cartesian grid. The wall function derived directly from Spalart-Allmaras (S-A) turbulence model or its modified version is employed to determine proper tangential velocity boundary condition. Several two-dimensional (2-D) cases, such as non-inclined / inclined flat plate, zero attack NACA 0012 airfoil, are investigated to check the accuracy of the present IBM. Although the skin friction coefficients are very difficult to predict, the surface pressure coefficient of the airfoil can be calculated accurately even with a coarse grid, in which the y^+ of the reference point defined at leading edge is about 501.9. Compared to the original wall function, the modified wall function achieves a better grid convergence. The validation cases of plate and NACA 0012 have shown the primary ability of the present IBM to treat attached flow.

INTRODUCTION

Although body-conformal grids, structured or unstructured, have been widely used in Computational Fluid Dynamics (CFD) to simulate flows around arbitrary bodies, the automatic grid generation or reconstruction is still a big challenge when dealing with complex or moving geometry. Therefore, the Cartesian grid methods, which can generate the grid automatically and rapidly around complex solid boundaries, have come back to the lime-light. In the simplest Cartesian grid method, boundaries are generally approximated as a series of staircase-like steps, which would introduce deviations into the solution (Ferziger and Peric, 2012). In order to reproduce the wall boundary smoothly and accurately in Cartesian grid solvers, three primary methods have been applied: the hybrid grid method (Charlton, 1997, Wang, 1998), the cut-cell method (Lee and Ruffin, 2007, Harada *et al.*, 2017) and the immersed boundary methods (Mittal and Iaccarino, 2005, Du *et al.*, 2014, Du and Sun, 2015). When the layer grids are used along with the Cartesian grids in a hybrid grid method, the boundary layer is easily treated as commonly used body-conformal grids. However, the laborious grid generation and complicated coordinate transformation and interpolation are required again (Lee and Ruffin, 2007). The cut-cell methods cut the cells that intersect with wall surfaces. The cut-cell method can track the boundary as exact as body-conformal grids, whereas the calculation of the intersection is complicated, and special treatments such as cell-merged techniques are required to handle the small cells in the vicinity of the geometry (Udaykumar *et al.*, 2001). On the other hand, the IBM uses only orthogonal cells, and sharp interface can also be achieved straightforward (Du et al., 2014, Majumdar *et al.*, 2001), it is a simple and robust method.

Adaptive grid refinement technique has been proved to be a promising approach to enhance the local grid resolution only at interested regions, such as near the boundary or with high gradient, and have been validated in incompressible / compressible laminar flow. With the help of local grid refinement, Tullio et al. (de Tullio *et al.*, 2007) have also proved that simulation of a turbulent boundary layer is possible if the minimum cell size is smaller than the height of the viscous sublayer. However, the isotropic property of Cartesian grid will significantly increase near wall grid density, which will become fatal when the Reynolds number becomes higher. Therefore, two distinct wall treatments have been proposed to alleviate the grid resolution constraint of High-Reynolds simulation.

The first treatment is to take advantage of the wall function methods to bridge the near wall region to core region of the turbulence with analytical expressions, which are derived from turbulent boundary layer function. Ghosh et al. (Ghosh *et al.*, 2010) used a power-law expression along with a discrete continuity equation to reconstruct the velocity vector at near wall grid. Lee and Ruffin (Lee and Ruffin, 2007) used Spalding's formulation, which yields a unified form valid for the log law layer and the viscous sublayer as well as the buffer layer, to determine the tangential velocity at the ghost cell. Kalitzin et al. (Kalitzin *et al.*, 2005) suggested to build adaptive wall functions based on well-resolved numerical look-up tables for each individual turbulent model to ensure consistency between the eddy-viscosity and the velocity gradient. Recent years, in the re-searches team of University of Tokyo (Tamaki *et al.*, 2017, Harada et al., 2017), following the advice of Kalitzin, a new SA wall model (Allmaras and Johnson, 2012) is served as a

specific wall function for the SA turbulence model and a linear relation between local modified eddy-viscosity $\tilde{\upsilon}$ and non-dimensional length y^+ is used to define the boundary condition for the turbulent simulation.

The second treatment is the two-layer wall models, which are originally developed to replace the near-wall region with a wall model (a set of boundary-layer equations) to provide approximate wall boundary conditions for outer large eddy simulation (LES) in body-conformal grid. Tessicini et al. (Tessicini *et al.*, 2002) have validated the applicability of a simple near-wall model, based on the local equilibrium hypothesis, in the framework of IB method for LES. Capizzano (Capizzano, 2011) have solved the Reynolds-averaged Navier–Stokes (RANS) equations on external region and simplified layer equations (Wang and Moin, 2002) on embedded virtual subgrid that originates from the forcing point down to the solid surface near the wall. A slip velocity has been assigned to ensure the correct wall-shear. Indeed, the two-layer wall model is expected to be more accurate in the application of separated flow and unsteady flow, on account of the capability of boundary-layer equations in considering the effect of unsteady and convection.

In order to simulate turbulent flows in Cartesian grid, a sharp immersed boundary method using a wall function to describe the boundary layer has been developed. Firstly, the numerical method employed will be discussed, including the governing equations, grid generation and wall function implement. Then, three 2-D cases will be studied to validate the sharp IBM, including the non-inclined plate, inclined plate and the NACA 0012 airfoil with zero attack. Both the distribution of skin friction coefficient and the profile of tangential velocity are investigated by using different wall functions. Finally, a comprehensive conclusion for the sharp IBM is given.

NUMERICAL METHODS

In the past few years, our group (Du et al., 2014, Du and Sun, 2015) has validated our sharp interface IBM thoroughly for simulating both stationary and moving boundary problems (i.e. vortex-induced vibration) in compressible flow using stretched grid. Nowadays, in order to extend our inhouse code's ability in handling complex geometry and high-Reynolds flow, wall function method have been investigated.

Governing equations

The 2-D unsteady compressible Reynolds-averaged Navier–Stokes equations are written in terms of conservative variables:

$$\begin{aligned}
&\frac{\partial \rho}{\partial t}+\frac{\partial(\rho u_j)}{\partial x_j}=0,\\
&\frac{\partial(\rho u_i)}{\partial t}+\frac{\partial(\rho u_i u_j)}{\partial x_j}+\frac{\partial p}{\partial x_i}-\frac{\partial \tau_{ij}}{\partial x_j}=0,\\
&\frac{\partial E}{\partial t}+\frac{\partial(E u_j+p u_j)}{\partial x_j}-\frac{\partial(\tau_{ij}u_i-q_j)}{\partial x_j}=0,
\end{aligned} \tag{1}$$

where ρ represents the density, p represents the pressure, u_i represents the velocity component in the i-*th* coordinate direction (i = 1,2), E represents the total energy per unit volume. The total energy is given by:

$$E=\frac{p}{\gamma-1}+\frac{1}{2}\rho u_i u_i, \tag{2}$$

where γ denotes the specific heat capacity ratio. The total stress tensor τ_{ij} is the sum of the viscous and the Reynolds stress tensor:

$$\tau_{ij}=2\rho(\upsilon+\upsilon_t)S_{ij}^{*}, \qquad S_{ij}^{*}=S_{ij}-\frac{1}{3}S_{kk}\delta_{ij}, \tag{3}$$

where the Boussinesq hypothesis is applied through the introduction of the eddy viscosit υ_t, and where $S_{ij}=(u_{i,j}+u_{j,i})/2$ is the strain-rate tensor, υ the molecular viscosity, depending on temperature T through Sutherland's law. Similarly, the total heat flux q_j is the sum of a molecular and a turbulent contribution:

$$q_j=-\rho c_p\left(\frac{\upsilon}{\mathrm{Pr}}+\frac{\upsilon_t}{\mathrm{Pr}_t}\right)\frac{\partial T}{\partial x_j}, \tag{4}$$

Pr, Pr_t are the molecular and turbulent Prandtl numbers, assumed to be 0.72 and 0.9, respectively.

S-A turbulent model (Spalart and Allmaras, 1992), which only solves a transport equation of the modified eddy-viscosity $\tilde{\upsilon}$, is employed to achieve turbulence closure:

$$\begin{aligned}
&\frac{\partial \rho\tilde{\upsilon}}{\partial t}+\frac{\partial(\rho\tilde{\upsilon}u_j)}{\partial x_j}=\\
&\qquad(\text{Production})-(\text{Destruction})+(\text{Diffusion}),
\end{aligned} \tag{5}$$

where the production term, destruction term and diffusion term are defined as:

$$\begin{aligned}
&(\text{Production})=c_{b1}(1-f_{t2})\rho\tilde{S}\tilde{\upsilon},\\
&(\text{Destruction})=[\rho c_{w1}f_w-\rho\frac{c_{b1}}{\kappa^2}f_{t2}](\frac{\tilde{\upsilon}}{d})^2,\\
&(\text{Diffusion})=\frac{1}{\sigma}[\frac{\partial}{\partial x_j}((\rho\upsilon+\rho\tilde{\upsilon})\frac{\partial\tilde{\upsilon}}{\partial x_j})+c_{b2}\rho\frac{\partial\tilde{\upsilon}}{\partial x_i}\frac{\partial\tilde{\upsilon}}{\partial x_i}],\\
&f_{v1}=\frac{\chi^3}{\chi^3+c_{v1}^3}, \quad \chi=\frac{\tilde{\upsilon}}{\upsilon}, \quad f_{t2}=c_{t3}\exp\left(-c_{t4}\chi^2\right)\\
&\tilde{S}=\Omega+\frac{\tilde{\upsilon}}{\kappa^2 d^2}f_{v2}, \quad \Omega=\frac{1}{2}\sqrt{(\frac{\partial u_i}{\partial x_j}-\frac{\partial u_j}{\partial x_i})^2},\\
&f_{v2}=1-\frac{\chi}{1+\chi f_{v1}}, \quad f_w=g\left[\frac{1+c_{w3}^6}{g^6+c_{w3}^6}\right]^{1/6},\\
&g=r+c_{w2}\left(r^6-r\right), \quad r=\min\left[\frac{\tilde{\upsilon}}{\tilde{S}\kappa^2 d^2},10\right],
\end{aligned} \tag{6}$$

with d refer to the wall distance of the grid. The other constants in the model are as follow:

$$c_{b1}=0.1355\,,\quad \sigma=2/3\,,\quad c_{b2}=0.622\,,$$
$$\kappa=0.41\,,\quad c_{w2}=0.3\,,\quad c_{w3}=2\,,$$
$$c_{v1}=7.1\,,\quad c_{t3}=1.2\,,\quad c_{t4}=0.5\,,$$
$$c_{w1}=\frac{c_{b1}}{\kappa^2}+\frac{1+c_{b2}}{\sigma}\,,$$

then, the eddy viscosity can be obtained as: $\upsilon_t=\tilde{\upsilon}f_{v1}$. Second-order central difference scheme in space and third order Runge-Kutta time integration are used to solve the RANS equations.

The S-A turbulent model permit the following simple linear solution for $\tilde{\upsilon}$ near the wall:

$$\tilde{\upsilon}=\kappa u_\tau d\quad , \tag{7}$$

where u_τ represents the shear stress velocity. To ensure the consistency between the wall function and the turbulence function, a new analytic solution (Allmaras and Johnson, 2012) of tangential velocity derived directly from the S-A turbulence model is employed as the wall function, which is applicable down to the viscous sublayer:

$$\begin{aligned}u^+\left(y^+\right)=&\bar{B}+c_1\log\left(\left(y^++a_1\right)^2+b_1^2\right)-\\ &c_2\log\left(\left(y^++a_2\right)^2+b_2^2\right)-c_3\mathrm{ArcTan}\left(y^++a_1,b_1\right)-\\ &c_4\mathrm{ArcTan}\left(y^++a_2,b_2\right)\,,\end{aligned} \tag{8}$$

where nondimensional velocity and length are defined as $u^+=u/u_\tau$ and $y^+=u_\tau d/\upsilon$, respectively, and $\mathrm{ArcTan}\left(x,y\right)$ is the Mathematica function equivalent to the Fortran function $\mathrm{atan2}\left(y,x\right)$. The constants are given by,

$$\bar{B}=5.0333908790505579\,,$$
$$a_1=8.148221580024245\,,\quad b_1=7.4600876082527945\,,$$
$$a_2=-6.9287093849022945\,,\quad b_2=7.468145790401841\,,$$
$$c_1=2.5496773539754747\,,\quad c_2=1.3301651588535228\,,$$
$$c_3=3.599459109332379\,,\quad c_4=3.6397531868684494\,,$$

and Figure 1 shows the shape of the Eq. (8).

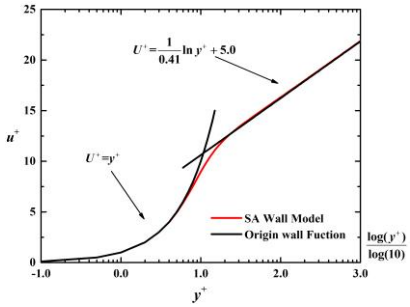

Figure 1 Velocity profile of the SA wall model

Grid Generation

The adaptive grid refinement method based on the given distance criterion, as shown in the Figure 2, has been developed to replace the original stretched grid by our group. Grid becomes finer when it gets closer to the wall boundary without increasing grid density at other area. Detail of the related algorithms and validations can be found in the work of Wang (Wang *et al.*, 2019). Here, a brief instruction of the grid generation will be given.

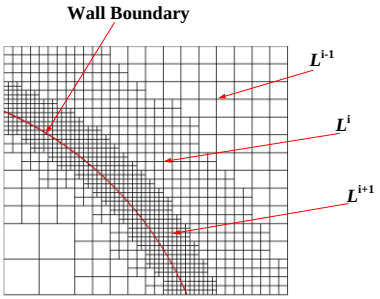

Figure 2 Adaptive grid refinement around arbitrary wall. The solid line in red represents the wall boundary.

The grid system consists of various Cartesian grid level with varying resolution. Assuming that L^i and Δx^i, i= 0,1,2,…, represent the individual grid level and their corresponding grid size, respectively:

$$\Delta x_i=\frac{\Delta x_0}{2^i}\,, \tag{9}$$

Where the subscript index 0 represent the initial background Cartesian grid, with Δx_0 being the corresponding grid size. G is the set of whole grid system, it can be defined as:

$$G=\sum_{i=0}L^i\,, \tag{10}$$

Firstly, a coarsest structured Cartesian grid level, L^0, is initialled to cover the whole computational domain, and the total grid number of L^0 is N^0. Then, the off-wall distance of each grid node d_i^0 $(i=1,2\cdots N^0)$ is calculated and a portion of grids which fulfill the given criterion, $d_i^0<D^0$, is marked. The new refined level, L^1, is generated by bisection of the marked L^0 grids at each direction. This refinement process is done iteratively, until an assigned target value is reached at the immersed boundary. Fully unstructured arrays are employed to store the locations, connection and refinement relations and physical variables of the whole refined grids. A time refinement is also proposed to get a constant CFL number in different grid refined layer:

$$\frac{\Delta t_i}{\Delta x_i}=\text{constant}\,, \tag{11}$$

Where Δt_i is the time step used on L_i.

Immersed Boundary Method

Present sharp IB method is originally developed for low-Reynolds flow (Du et al., 2014), in which the velocity boundary condition is imposed implicitly by reconstructing the velocity vector at the boundary points P_0 as shown in Figure 3.

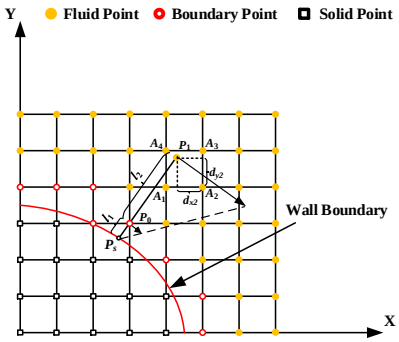

Figure 3 Schematic of a sharp immersed boundary in laminar flow. Solid Point is the point lying in the solid. Boundary point is the point lying in the fluid but connects at least one solid point. Fluid point is the point lying far from the wall boundary.

The line $\overline{P_s P_1}$ is across point P_0 and perpendicular to the solid surface at point P_s. Point P_1 is surrounded by four fluid grids $A_{1,2,3,4}$, from which the bilinear interpolation can be used to obtain the velocity vector of P_1:

$$\overrightarrow{V_{P_1}} = \sum_{i=1}^{4} \delta\left(\frac{d_{xi}}{\Delta x_{\min}}\right)\left(\frac{d_{yi}}{\Delta x_{\min}}\right)\overrightarrow{V_{A_i}}, \tag{12}$$

where the delta function is defined as:

$$\delta(x) = \begin{cases} 1-|x|, & |x|<1 \\ 0, & |x|\geq 1 \end{cases}, \tag{13}$$

here, $\Delta x_{\min}$ denotes the grid size near the wall boundary, d_{xi} and d_{yi} represent distances between point P_1 and i-th adjacent grid in the x- and y- direction, respectively. Then, the velocity at P_1 can be calculated through the linear interpolation:

$$\overrightarrow{V_{P_0}} = \frac{l_1}{l}\overrightarrow{V_{P_1}} + \frac{l_2}{l}\overrightarrow{V_{P_s}}, \tag{14}$$

where l_1 is the distance between points P_0 and P_s, and l_2 is the distance between points P_1 and P_0, $l = l_1 + l_2$, which is equal to $3\Delta x_{\min}$.

Although a similar interpolation procedure with more interpolation points has been validated by Tullio et al. (de Tullio et al., 2007) to simulate high-Reynolds flow, the linear interpolation can only be utilized in the viscous sublayer, this is a too strict confinement for the IBM, especially for the flow simulations involve complex geometries with curved and planar boundaries oblique to the grid. Therefore, wall function methods have been introduced to replace the original interpolation procedure for turbulent flow. Although the wall function always assumes incompressible wall, it can be extended to a compressible flow directly if the freestream Mach numbers is smaller than 1.4, which had been test numerically by Knopp et al. (Knopp *et al.*, 2006).

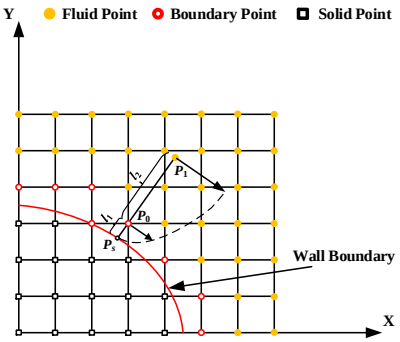

Figure 4 Schematic of a sharp immersed boundary in turbulent flow.

Original Wall Function

Figure 4 shows the schematic of the wall function method. Here, only the fluid cells (marked with solid circle) are solved directly from Eq. (1) and Eq. (5) and the boundary condition is imposed implicitly onto the boundary points. For each boundary point P_0, a corresponding reference point P_1 is set in the flow region. The location and state vector of the reference point P_1 are calculated by the same procedure illustrated in the laminar case. After getting the velocity vector of P_1, a coordinate transformation is employed to obtain the tangential u_{t,P_1} and normal velocity u_{n,P_1}. Then, substitute the u_{t,P_1} and wall distance $l = l_1 + l_2$ into Eq. (8):

$$u^+_{t,P_1} = f_{SA}\left(y^+_{p_1}\right), \quad u^+_{t,P_1} = \frac{u_{t,P_1}}{u_\tau}, \quad y^+_{P_1} = \frac{u_\tau l}{\upsilon}, \tag{15}$$

where f_{SA} represents the expression of Eq. (8). Then, u_τ can be solved using the Newton iterations. It is noted that a new expression of local Reynolds number Re_y can be obtained by multiplying both sides of Eq. (8) with y^+:

$$\mathrm{Re}_y \equiv du/\upsilon = y^+ f_{SA}\left(y^+\right) = F\left(y^+\right), \tag{16}$$

inverting this function gives an explicit expression of u_τ:

$$u_\tau = \frac{\upsilon}{d} F^{-1}\left(\mathrm{Re}_y\right), \tag{17}$$

learning from the experience of Kalitzin et al. (Kalitzin et al., 2005), this inversion can be performed once and for all and store the inverse function in a look-up table generated with the Eq. (8). Then, the calculated u_τ is used to determine the tangential velocity at the boundary point P_0:

$$u_{t,P_0} = f_{SA}\left(y^+_{P_0}\right)u_\tau, \quad y^+_{P_0} = \frac{u_\tau l_1}{\upsilon}, \tag{18}$$

for the adiabatic boundary condition, the temperature of P_0 can computed from Crocco-Busemann formula:

$$T_{P_0} = T_{P_1} + \frac{\mathrm{Pr}^{1/3}}{2c_p}\left(u^2_{t,P_1} - u^2_{t,P_0}\right), \tag{19}$$

the pressure of P_0 is equal to that of P_1:

$$P_{p_0} = P_{p_1} \ . \tag{20}$$

Here, a linear interpolation is used to obtain the wall-normal velocity component of P_0 for the non-penetrating boundary condition. Although different interpolation schemes had been adopted by researchers, such as: linear interpolation, bilinear interpolation and linear-quadratic (Majumdar *et al*., 2001), power-law (Ghosh *et al*., 2010), quadratic interpolation (Bernardini *et al*. 2016), none of the studies has shown that sophisticated interpolation schemes are significantly better than simple linear interpolation.

$$u_{n,P_0} = \frac{l_1}{l} u_{n,P_1} \tag{21}$$

Finally, Eq. (7) is used to calculate the $\tilde{\upsilon}$ of P_0:

$$\tilde{\upsilon}_{P_0} = \kappa u_\tau l_1 \tag{22}$$

Modified Wall Function

Tamaki et al. (Tamaki et al., 2017) has indicated that the unbalanced flux between the fluid cell and boundary cell is the primary factor to cause the oscillation in the surface pressure and fail to predict the proper friction coefficient. In order to resolve the near wall velocity correctly and maintain flux balance, the 'slip' boundary condition is introduced with a modified eddy viscosity profile. This method is now adopted to combine with our IBM directly. In present work, the wall distance l of reference point P_1 is served as the cut-off distance, below which a linear velocity profile is assumed. Meanwhile, the eddy viscosity profile under cut-off distance is also modified to be $\upsilon_t = const.$, maintaining the balance of shear stress.

The modified tangential velocity of point P_0 is defined as:

$$u_{t,P_0} = u_{t,P_1} - \left\{ \frac{\partial f_{SA}}{\partial y^+}\left(y_{P_1}^+\right) \right\} \left(y_{P_1}^+ - y_{P_0}^+ \right) u_\tau \ , \tag{23}$$

here, the $\partial f_{SA} / \partial y^+$ represents the first derivative of the Eq. (8). The other variables of P_0 is calculated from original formulae (18)-(21). But the shear stress at the grids below cut-off distance is obtained by:

$$\tau = \rho u_\tau^2 \ , \tag{24}$$

to obtain the constant υ_t from a linear solution of $\tilde{\upsilon}$, the damping function $f_{\upsilon 1}$ in the S-A model is reconstructed as a new one $f'_{\upsilon 1}$:

$$\begin{aligned} f'_{\upsilon 1} &= f_{\upsilon 1,w} f_e + f_{\upsilon 1}(1 - f_e) \ , \\ f_{\upsilon 1,w} &= r_d \frac{(\chi r_d)^3}{c_{\upsilon 1}^3 + (\chi r_d)^3} \ , \\ f_e &= 0.5 + 0.5 \tanh\left\{ c_e (1 - \frac{1}{r_d}) \right\}, \qquad c_e = 5 \ , \end{aligned} \tag{25}$$

where $r_d = d_{p_1} / d$. The new damping function $f'_{\upsilon 1}$ is the product of r_d and original $f_{\upsilon 1}$ at P_1.

VALIDATION RESULT

Several representative numerical results are presented here as the preliminary validation cases to illustrate the primary ability of the present IBM to treat attached flow.

Flat Plate

In this section, turbulent flow simulations are performed by solving the flows around a two-dimensional thin flat plate at $\mathrm{Mach}_\infty = 0.2$ and $\mathrm{Re}_\infty = 1.0 \times 10^6$. To preliminarily investigate the accuracy of the results for the nonaligned grids, the flat plate is inclined by θ (deg) relative to the grids. The orientation angle θ is set to 0 and 15 degree, as shown in Figure 5. The chord length of the plate is $c = 2.0$, while the reference length for the Reynolds number is 1.0, and the thickness of the plate is 0.002 with a cylindrical leading and trailing edge. Both the inhouse IBM solver and a commercial CFD solver (i.e. Fluent) have been used to calculate this problem. The settings of the computational meshes are described in Table 1. In Table 1 (also the Table 2), the y^+ of IBM is calculated at the reference points, while for Fluent y^+ is defined at first off-wall cell. The refinement levels for the IBM is kept 5 for all cases. Both the original and modified wall functions have been used in the IBM.

Table 1 Characteristics of the computational meshes for turbulent flat plate

			Minimize grid size: $\Delta x_{\min}$	y^+
Fluent			1.0×10^{-5}	0.2
IBM	α=0° (Case 1)	Coarse	2.0×10^{-3}	267.6
		Medium	1.4×10^{-3}	182.7
		Fine	8.0×10^{-4}	106.8
	α=15° (Case 2)	Coarse	2.0×10^{-3}	275.7
		Medium	1.4×10^{-3}	192.3
		Fine	8.0×10^{-4}	110.7

Case 1

Figure 5a gives a sketch of this case. Figure 6 shows the distribution of skin friction coefficient $c_f = \tau_w / (1/2 \rho u_\infty^2)$ on the flat plate. The results obtained by modified wall function have shown the similar trend as that obtained by the original wall function. As shown in Figure 6a, an unexpectedly increase of c_f along the whole chord of plate is observed with the fine grid, $y^+ = 110.7$. The y^+ result of fine grid implies that the most of first off-wall grid is locating in the buffer sub-layer, in which a large gradient of velocity is existing and cannot be resolved correctly with a numerical scheme with second-order spatial accuracy (Tamaki et al., 2017).

Although small deviation exists as the grid resolution increasing, a relatively converged solution of c_f can be obtained (Figure 6b) with the modified wall function in the whole calculated y^+ region. The grid convergence of nondimensional tangential velocity with different wall function are shown in Figure 7. The considerable agreement with the result of Fluent is achieved for both wall function with different grid resolution, but the performance of modified wall function is still better than that of the original one.

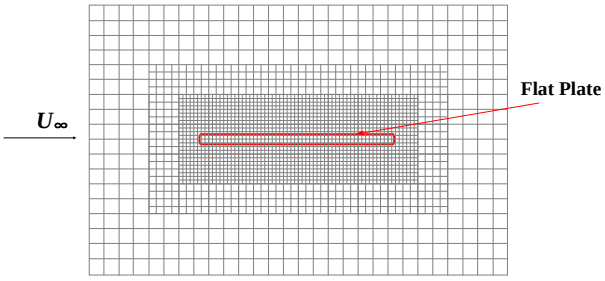

(a) $\alpha = 0^\circ$

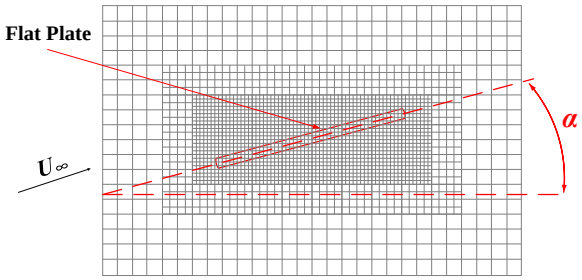

(b) $\alpha = 15^\circ$

Figure 5 Illustration of flow simulation around a flat plate

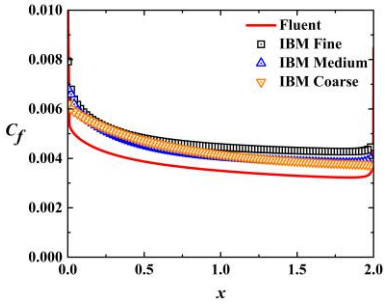

(a) Original Wall Function

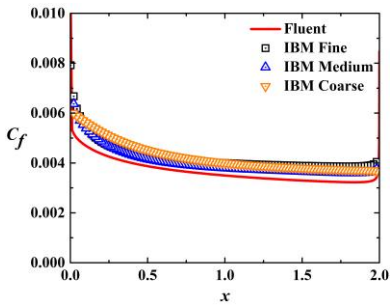

(b) Modified Wall Function

Figure 6 Skin friction coefficient of plate with $\alpha = 0^\circ$

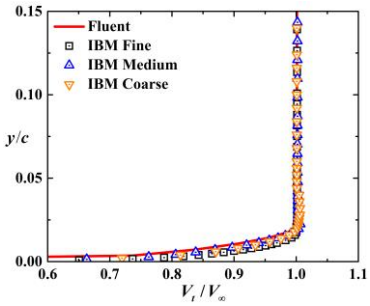

(a) Original Wall Function

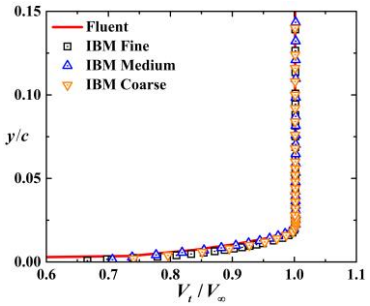

(b) Modified Wall Function

Figure 7 Tangential velocity of plate with $\alpha = 0^\circ$

Case 2.

Figure 5b gives a sketch of this case. Figure 8a shows the results of skin friction coefficient obtained by original wall function. Compared to the result in Figure 6a, it is no surprised to find that a large deviation is emerged when plate is not aligned with the Cartesian grids. Similar results have also been reported by other researchers (Harada et al., 2017). What's more, the grid convergence of the IBM with original wall function is destroyed completely when the plate is inclined. In contrast, modified wall function does not severely mispredict skin friction when the plate is inclined, and a notable converged result is obtained by the modified wall function, as shown in Figure 8b. The grid convergence of nondimensional tangential velocity for $\alpha = 15^\circ$ is presented in Figure 9. Similarly, a better grid convergence is achieved by using modified wall function.

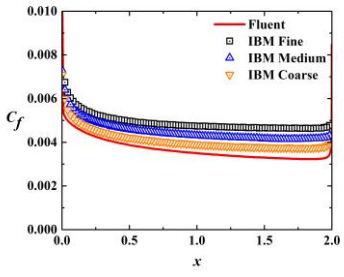

(a) Original Wall Function

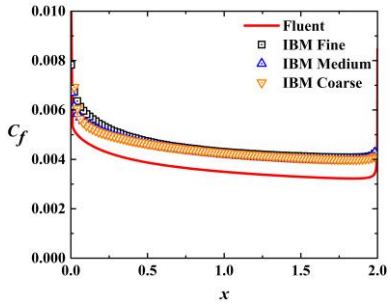

(b) Modified Wall Function

Figure 8 Skin friction coefficient of plate wit $\alpha = 15^\circ$

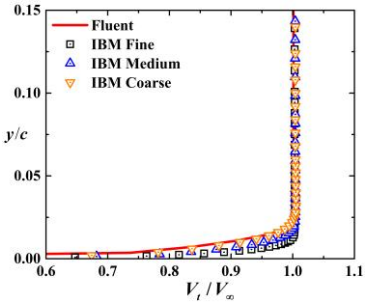

(a) Original Wall Function

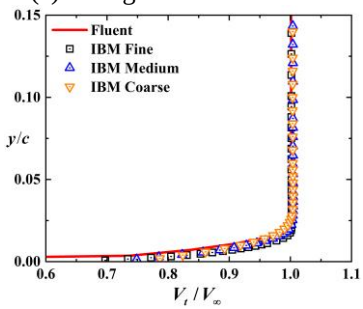

(b) Modified Wall Function

Figure 9 Tangential velocity of plate with $\alpha = 15^\circ$

NACA 0012

In this section, turbulent flow simulations are performed by solving the flows around a 2-D low-subsonic NACA 0012 airfoil at $\text{Mach}_\infty = 0.3$ and $\text{Re}_\infty = 3\times10^6$ with zero angle incidence, which has been calculated by Capizzano et al. (Capizzano, 2011). The body fitted results extracted from their work serve as the reference values in this section. In present work, a computational domain extending 40c away from the body is initially discretized using a uniform Cartesian with $\Delta x_0 = 0.5c$. Four different refinement levels are adopted, i.e. 8, 9, 10, 11 (represent as rf = 8, 9, 10, 11, respectively). The detail information of the calculated grid is summarized in Table 2.

Figure 10 shows the distribution of pressure coefficient C_p on NACA 0012. The results of two wall function both match well with that of body fitted grid. Different from the C_p, the distribution of the C_f shown in Figure 11 deviates from the result of body fitted, especially for the original wall function. For the modified wall function, a relatively converged C_f is achieved before using the finest grid. The y^+ of the finest grid is 86.4, which implies that most part of the first off-wall grid above the airfoil locate in the buffer sub-layer as illustrate in the last section. What's more, with the improvement of grid resolution, the maximum value of C_f at the leading edge can be captured by IBM.

Table 2 Characteristics of the computational meshes for NACA 0012 airfoil

Refinement Level	$\Delta x_{\min}$	y^+
8	1.95×10^{-3}	501.9
9	9.76×10^{-4}	288.7
10	4.88×10^{-4}	166.1
11	2.44×10^{-4}	86.4

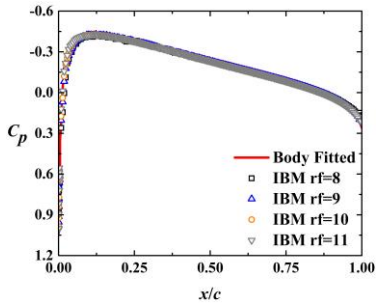

(a) Original Wall Function

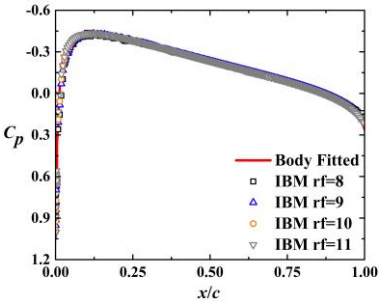

(b) Modified Wall Function

Figure 10 Distribution of C_p on NACA 0012

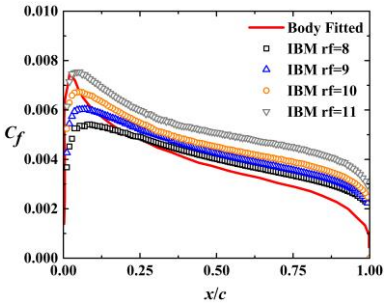

(a) Original Wall Function

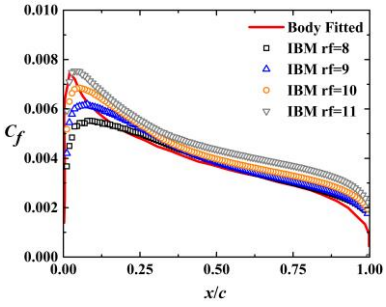

(b) Modified Wall Function

Figure 11 Distribution of C_f on NACA 0012

CONCLUSIONS

In order to simulate turbulent flow around complex geometries, a sharp immersed boundary method using finite difference algorithm has been developed. A new wall function directly derived from Spalart-Allmaras turbulence model or its modified version developed by Tokyo university research team is employed to avoid the sharp increment of the grid number required to resolve a turbulent boundary layer. The 2-D cases of the non-inclined / inclined flat plate and zero attack NACA 0012 prove the primary ability of the present IBM to treat attached flow. Whether flat plate is inclined or non-inclined, the IBM using a modified wall function can achieve converged results with the y^+ defined at the reference point varying from 100 to 260. Although there still exist certain deviations in the results of modified wall function, it has demonstrated obvious advantages in the grid convergence and the accuracy of prediction, comparing to the original wall function. In the case of NACA 0012 with zero attack, the surface pressure coefficient of the airfoil can be calculated accurately even with a rather coarse grid, in which the y^+ of reference point defined at leading edge is about 501.9. In order to further improve the calculation accuracy of IBM in turbulent simulations, more attention should be payed to maintain the conservation property at the interface around the immersed boundary, and the two-layer wall model should also be taken into consideration.

ACKNOWLEDGMENTS

Financial support from the National Science Foundation of China (Grants No. 51790514 and 51706006) is gratefully acknowledged.

REFERENCES

ALLMARAS, S. R. & JOHNSON, F. T. (2012), "Modifications and clarifications for the implementation of the Spalart-Allmaras turbulence model", in Seventh international conference on computational fluid dynamics (ICCFD7), pp. 1-11.

Bernardini, M., Modesti, D., & Pirozzoli, S. (2016), "On the suitability of the Immersed Boundary method for the simulation of high-Reynolds-number separated turbulent flows", Computers and Fluids, Vol. 130, pp. 84-93.

CAPIZZANO, F. (2011), "Turbulent Wall Model for Immersed Boundary Methods", AIAA Journal, Vol. 49, No. 11, pp. 2367-2381.

CHARLTON, E. F. (1997) An Octree Solution to Conservation-laws over Arbitrary Regions (OSCAR) with Applications to Aircraft Aerodynamics., University of Michigan.

De TULLIO, M. D., De PALMA, P., IACCARINO, G., PASCAZIO, G. & NAPOLITANO, M. (2007), "An immersed boundary method for compressible flows using local grid refinement", Journal of Computational Physics, Vol. 225, No. 2, pp. 2098-2117.

DU, L. & SUN, X. (2015), "Suppression of vortex-induced vibration using the rotary oscillation of a cylinder", Physics of Fluids, Vol. 27, No. 2.

DU, L., JING, X. & SUN, X. (2014), "Modes of vortex formation and transition to three-dimensionality in the wake of a freely vibrating cylinder", Journal of Fluids and Structures, Vol. 49, pp. 554-573.

FERZIGER, J. H. & PERIC, M. (2012), Computational methods for fluid dynamics, Springer Science & Business Media

GHOSH, S., CHOI, J. & EDWARDS, J. R. (2010), "Numerical Simulations of Effects of Micro Vortex Generators Using Immersed-Boundary Methods", AIAA Journal, Vol. 48, No. 1, pp. 92-103.

HARADA, M., TAMAKI, Y., TAKAHASHI, Y. & IMAMURA, T. (2017), "Simple and Robust Cut-Cell Method for High-Reynolds-Number-Flow Simulation on Cartesian Grids", AIAA Journal, 2833-2841.

KALITZIN, G., MEDIC, G., IACCARINO, G. & DURBIN, P. (2005), "Near-wall behavior of RANS turbulence models and implications for wall functions", Journal of Computational Physics, Vol. 204, No. 1, pp. 265-291.

Knopp, T., Alrutz, T., & Schwamborn, D. (2006). "A grid and flow adaptive wall-function method for RANS turbulence modelling". Journal of Computational Physics, Vol. 220, No.1, pp. 19-40.

LEE, J. D. & RUFFIN, S. (2007), "Development of a Turbulent Wall-Function Based Viscous Cartesian-Grid Methodology", in 45th AIAA Aerospace Sciences Meeting and Exhibit, Reno, Nevada.

MAJUMDAR, S., IACCARINO, G. & DURBIN, P. (2001), "RANS solvers with adaptive structured boundary non-conforming grids", Annual Research Briefs, Center for Turbulence Research, Stanford University, 353-466.

MITTAL, R. & IACCARINO, G. (2005), "Immersed boundary methods", Annu. Rev. Fluid Mech., Vol. 37, pp. 239-261.

SPALART, P. & ALLMARAS, S. (1992), "A one-equation turbulence model for aerodynamic flows", in 30th aerospace sciences meeting and exhibit.

TAMAKI, Y., HARADA, M. & IMAMURA, T. (2017), "Near-wall modification of Spalart–Allmaras turbulence model for immersed boundary method", AIAA Journal, 3027-3039.

TESSICINI, F., IACCARINO, G., FATICA, M., WANG, M. & VERZICCO, R. (2002), "Wall modeling for large-eddy simulation using an immersed boundary method", Annual Research Briefs, 181-187.

UDAYKUMAR, H. S., MITTAL, R., RAMPUNGGOON, P. & KHANNA, A. (2001), "A Sharp Interface Cartesian Grid Method for Simulating Flows with Complex Moving Boundaries", Journal of Computational Physics, Vol. 174, No. 1, pp. 345-380.

WANG, M. & MOIN, P. (2002), "Dynamic wall modeling for large-eddy simulation of complex turbulent flows", Physics of Fluids, Vol. 14, No. 7, pp. 2043.

WANG, Z. J. (1998), "A Quadtree-based adaptive Cartesian/Quad grid flow solver for Navier-Stokes equations", Computers and Fluids, Vol. 27, No. 4, pp. 529-549.

WANG, Z., DU, L. & SUN, X. (2019) "Adaptive mesh refinement for simulating fluid-structure interaction using sharp interface immersed boundary method", Preparing to publish.